UJEAS

UNIZIK JOURNAL OF ENGINEERING AND APPLIED SCIENCES

UNIZIK Journal of Engineering and Applied Sciences 6(1), March (2026), 3185-3199
Journal homepage: https://journals.unizik.edu.ng/index.php/ujeas
PRINT ISSN: 2992-4383 || ONLINE ISSN: 2992-4391

Quadratic Drag–Based Modeling and Experimental Validation of Palm Nut Cracking and Separation Trajectories

Wilfred Chukwuemeka Mba[1], Sam Nna Omenyi[2], Ugochukwu Chuka Okonkwo[3], Nkemakonam Chidiebube Igbokwe[4] and Denis Chimeziri Onyekwere[5]
[1]Department of Automobile and Mechanical Technology Education, Federal College of Education (Technical), Umunze.
[2,3]Department of Mechanical Engineering, Nnamdi Azikiwe University, Awka
[4]Department of Industrial and Production Engineering, Nnamdi Azikiwe University, Awka
[5]Projects Development Institute, Enugu

Corresponding Author's E-mail: willymba.c@gmail.com

Abstract
Efficient separation of palm kernels from the shells remains a critical challenge in palm kernel oil processing, with conventional methods typically achieving inadequate separation efficiency. Traditional method which has high separation efficiency is however slow and labour-intensive. This study developed and experimentally validated a quadratic drag–based projectile motion model that predicted and optimized the post-cracking separation trajectories of palm nuts components in centrifugal cracking systems. The model incorporated particle-specific mass, geometry, drag coefficients, and air resistance effects, and was numerically solved for projection angles ranging from 10° to 45° and discharge velocities of 10 m/s and 15 m/s. Experimental trials were conducted using a fabricated centrifugal cracking and separation machine to validate the model predictions. Results show that separation effectiveness increases with both projection angle and velocity due to enhanced aerodynamic drag interaction. At 10 m/s, optimal separation was achieved between 30° and 40°, while at 15 m/s, a projection angle of 30° produced the clearest spatial separation with minimal space requirement. Under this optimal condition, kernel, nut, and shell deposition distances were 18.75 m, 17.44 m, and 13.72 m, respectively. Polynomial fits of displacement versus angle yielded excellent agreement with experimental data, with coefficients of determination ($R^2 \geq 0.995$). The study demonstrates that quadratic drag effects are essential for accurately predicting separation trajectories at practical operating speeds. The proposed model provides a physics-based separation principle (an alternative engineering approach to age-old processing steps), predictive framework for optimizing separator design and operating parameters (formulation of empirical models, for the first time, that could enable prediction of separation distances before the actual design application), thereby reducing reliance on empirical trial-and-error approaches in palm kernel processing systems.

Keywords: Quadratic projectile drag principle; Palm nut cracking and separation; Aerodynamic interaction.

1. Introduction

Palm kernel processing remains a critical unit operation in the palm oil value chain, particularly in Nigeria and other tropical economies where palm kernel oil is a major industrial feed stock for food, cosmetics, pharmaceutical and chemical industries (Alhaji et al., 2024; Amafade & Ovharhe, 2024; Shehu et al., 2021). A key bottleneck in this process is the efficient separation of cracked palm kernels from shells following mechanical cracking. Conventional separation approaches such as manual sorting, clay-water bath separation, screening, and air classification are either

labor-intensive, moisture-inducing, or limited in efficiency, typically achieving inadequate separation efficiency (Cao, 2023; Diepenbroek et al., 2024). Recent mechanized cracking systems increasingly rely on centrifugal impact, which ejects mixtures of kernels and shells into free flight. However, most existing studies analyze post-cracking separation using empirical observations or simplified projectile motion models that neglect aerodynamic drag (Alade et al., 2019; Bakri et al., 2020; Edeh et al., 2022; Man et al., 2023; Taofik et al., 2019). Such assumptions are inadequate for accurately predicting deposition distances of palm kernels and shells, which differ significantly in mass, geometry, and drag characteristics (Adepoju et al., 2023).

Previous studies have focused on empirical observations of deposition distances without rigorously applying or validating nonlinear theoretical models such as those involving quadratic air resistances. This study addresses this gap by developing and experimentally validating a quadratic drag–based projectile motion model to predict the separation trajectories of palm nuts, kernels, and shells.

2.0 Materials and methods

2.1 Materials and Physical Properties

Dried palm nuts of the ***Dura*** variety were sourced locally and conditioned to moisture contents consistent with typical processing conditions. After cracking, the mixture consisted of uncracked nuts, kernels, and shells. Representatively, physical properties (mass, size, shape, and sphericity) were adopted from standard literature (Eje, Chiwetalu and Ogbuagu, 2016) and validated by sampling. Mean particle masses were approximately 0.00186 kg for nuts, 0.00111 kg for kernels, and 0.00040 kg for shells, reflecting their distinct aerodynamic behaviors. Kernels were assumed nearly spherical, nuts elliptical, and shells shallow curved fragments, consistent with observed geometry during processing. Air density was taken as 1.225 kg/m³ under ambient laboratory conditions. Drag coefficients were selected based on particle shape: 0.47 for kernels, 0.8 for nuts, and 0.9 for shells, in line with established aerodynamic data for irregular agricultural particles.

2.2 Quadratic Drag Projectile Motion Model

The post-cracking separation process was modeled as projectile motion under gravity and quadratic air resistance. For each particle type, motion was described in two dimensions by coupled nonlinear differential equations in the horizontal and vertical directions. The drag force was assumed proportional to the square of velocity and acted opposite to the direction of motion. Gravity acted only in the vertical direction. The governing equations incorporated particle mass, drag coefficient, projected cross-sectional area, and instantaneous velocity. Initial conditions were defined by the discharge velocity and projection angle at the exit of the cracking chamber. Linear drag effects were neglected due to the moderate-to-high Reynolds number regime associated with ejection velocities of 10–15 m/s. The quadratic projectile drag equations used to formulate these numerical solutions are:

Trajectory Motion of the Particles

For motion in the x-direction

$F_{Dx} = -bV_x$
$m\ddot{x} = -b$

$$m\ddot{y} = -mg - b\dot{y} \quad (1.0)$$

$from\ eq\ 1$

$$\ddot{x} + \frac{b}{m}\dot{x} = 0 \quad (1.1)$$

$let\ x = e^{\lambda t}$

$\dot{x} = \lambda e^{\lambda t}\ and\ \ddot{x} = \lambda^2 e^{\lambda t}$

$substituting\ for\ \dot{x}\ and\ \ddot{x}\ in\ equation\ 3, we\ have$

$$\lambda^2 e^{\lambda t} + \frac{b}{m}\lambda e^{\lambda t} = 0 \quad (1.2)$$

$$\Rightarrow \lambda\left(\lambda + \frac{b}{m}\right) = 0$$

$The\ complimentary\ function\ of\ x\ (x_{cf})$

$$x_{cf} = A + Be^{\frac{-bt}{m}}$$

$$\Rightarrow \dot{x} = -\frac{b}{m}Be^{\frac{-bt}{m}} \qquad (1.3)$$

$$at\ t = 0, \qquad \dot{x}(0) = u_x$$

$$\Rightarrow u_x = -\frac{b}{m}B \Rightarrow B = -\frac{mu_x}{b}$$

$$at\ t = 0, \qquad x(0) = 0$$

$$\Rightarrow 0 = A + B$$

$$\Rightarrow A = \frac{mu_x}{b}$$

$$\Rightarrow x = \frac{mu_x}{b}(1 - e^{\frac{-bt}{m}}) \qquad (1.4)$$

For motion in the y-direction

$$F_{Dy} = -mg - bV_y$$

$$m\ddot{y} = -mg - b\dot{y} \qquad 1.5)$$

$$\ddot{y} + \frac{b}{m}\dot{y} = -g \qquad (1.6)$$

$The\ complimentary\ function\ of\ y\ (y_{cf})$

$$y_{cf} = A + Be^{\frac{-bt}{m}}$$

$The\ particular\ integral\ \ of\ y\ (y_{pi})$

$$y_{pi} = \alpha t^2 + \beta t$$

$$\Rightarrow 2\alpha + \frac{b}{m}(2\alpha t) + \frac{b}{m}\beta = -g \qquad (1.7)$$

let $\alpha = 0$ and compoaring the constant terms on both sides we have

$$\Rightarrow \frac{\mathrm{b}}{\mathrm{m}}\beta = -\mathrm{g}$$

$$\Rightarrow \beta = \frac{-\mathrm{mg}}{\mathrm{b}} \qquad (1.8)$$

Therefore, the overall solution for y will be complimentary function plus particular integral

$$y = A + Be^{\frac{-bt}{m}} - \frac{mgt}{b} \qquad (1.9)$$

$$\dot{y} = -\frac{b}{m}Be^{\frac{-bt}{m}} - \frac{mg}{b} \qquad (1.10)$$

$\dot{y}(0) = v$

$$\Rightarrow v = -\frac{b}{m}B - \frac{mg}{b} \quad (1.11)$$

$$B = -\frac{m}{b}\left(v + \frac{mg}{b}\right) \quad (1.12)$$

The quadratic projectile drag equations from equations (1. 3), (1.10), and (1.12) used to formulate these numerical solutions are:

$\dot{x}$=-$\frac{b}{m}Be^{\frac{-bt}{m}}$=$f_x(\dot{x}, \dot{y}, x, y)$

$\dot{y}$=-$\frac{b}{m}Be^{\frac{-bt}{m}}$-$\frac{mg}{b}$ =$f_y(\dot{x}, \dot{y}, x, y)$

B=-$\frac{m}{b}\left(v+\frac{mg}{b}\right)$

b=$\frac{A\rho C_D}{2m}$

$$\frac{d\dot{x}}{dt} = f_x(\dot{x}, \dot{y}, x, y) \quad (1.13)$$

$$\frac{d\dot{y}}{dt} = f_y(\dot{x}, \dot{y}, x, y) \quad (1.14)$$

$$\Rightarrow d\dot{x} = f_x(\dot{x}, \dot{y}, x, y)*dt \quad (1.15)$$

$$d\dot{y} = f_y(\dot{x}, \dot{y}, x, y)*dt \quad (1.16)$$

$Let\ f_x(\dot{x}, \dot{y}, x, y) = \kappa_x$

$f_y(\dot{x}, \dot{y}, x, y) = \kappa_y$

$At\ any\ time\ t_i, where\ i$=1,2,3 … … … …

$$\Rightarrow \dot{x}_{i+1} = \dot{x}_i + \kappa_{x_{(i)}}dt \quad (1.17)$$

$$\dot{y}_{i+1} = \dot{y}_i + \kappa_{y_{(i)}}dt \quad (1.18)$$

$Similarly,$

$$x_{i+1} = x_i + \dot{x}_{(i)}dt \quad (1.19)$$

$$y_{i+1} = y_i + \dot{y}_{(i)}dt \quad (1.20)$$

Where:

- C_D = drag coefficient (dimensionless),
- ρ = air density (kg/m³),
- A = cross-sectional area (m²),
- v = speed (m/s)

2.3 Numerical Solution Procedure

Due to the nonlinear nature of the quadratic drag equations, analytical solutions were not feasible. The equations of motion were therefore solved numerically using a time-stepping approach implemented in MATLAB. The trajectory of each particle type was computed until ground impact, and the horizontal deposition distance was recorded as the primary separation metric. Simulations were conducted for projection angles of 10°, 20°, 30°, 40°, and 45°, and for initial velocities of 10 m/s and 15 m/s, enabling systematic evaluation of separation trends.

2.4 Experimental Setup and Procedure

A centrifugal palm nut cracking and separation machine equipped with an adjustable discharge pipe was fabricated and used for experimental validation. The machine projected cracked mixtures onto a horizontal deposition platform. For each test condition, a known mass of dried palm nuts was fed into the machine, and the resulting nuts, kernels, and shells were allowed to follow free-flight trajectories.

Deposition distances were measured manually using a calibrated measuring tape. Each experiment was repeated three times, and mean separation distances were computed to reduce random measurement error

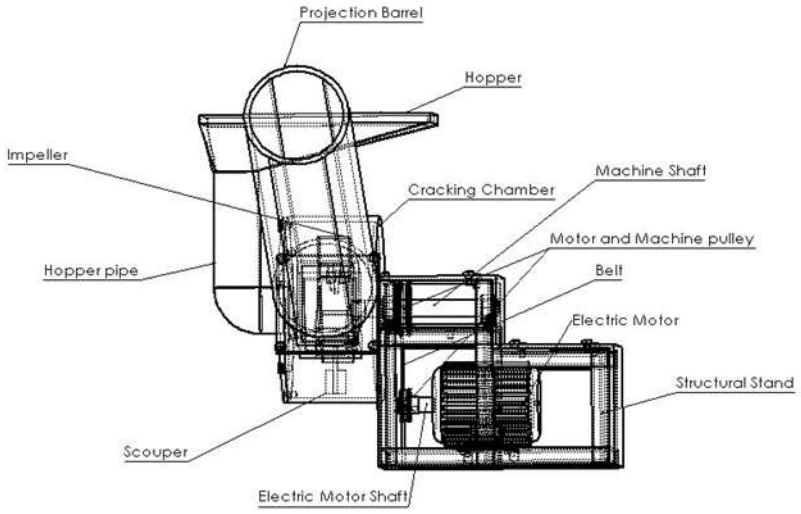

Plate 1.1a: Schematic Drawing of the Machine Assembly

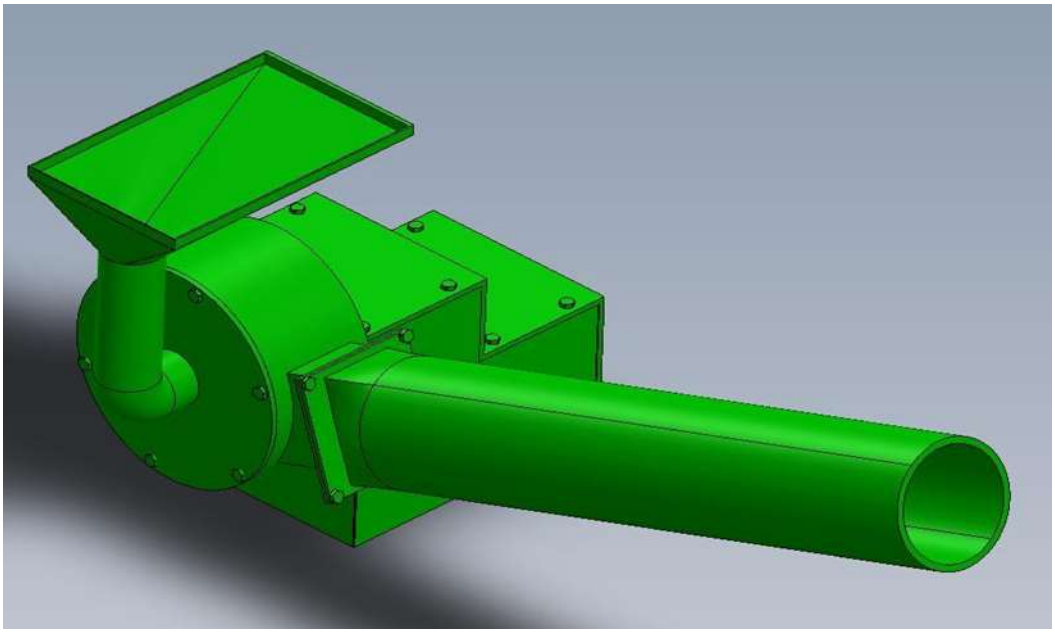

Plate 1.1b: Isometric Drawing of the Machine Assembly

2.5 Model Validation and Data Analysis

The numerical predictions of deposition distance were compared with experimental measurements to assess model validity. Deviations were attributed to frictional losses, particle–particle interaction, air turbulence, and variability in particle geometry. Separation efficiency was evaluated based on the spatial separation between kernel and shell deposition zones. The experimental results met theoretical expectations and align with relevant literatures. The trajectory ordering (kernel>nut>shell) was anticipated by drag physics and has been observed experimentally. The dependence on velocity and angle also matches the projectile motion formulas and prior tests. There is no contradiction; every key feature of the results of this study is supported either by fundamental equations or by analogous studies. Thus, the experiments as well as simulations are validated as correctly capturing the expected behaviours under quadratic drag.

3.0 Result and Discussion

The results obtained from simulating the projectile motion of palm nut components comprising the kernels, shells, and nuts under various launching angles and two velocities (10 m/s and 15 m/s) as depicted by the following graphs.

The motion trajectories of the kernels, shells, and nuts were plotted for launching angles of 10°, 20°, 30°, 40° and 45°. Each graph plotted y-displacement vs x-displacement, illustrating the flight paths under air drag conditions. At 10° (Fig. 1.1): The motion was mostly horizontal. All three components kernels, shells, and nuts landed close to each other, with minimal vertical displacement. Separation was poor due to similar low trajectories and limited time in air for drag to differentiate motion. At 20° (Fig. 1.2): A slight increase in vertical displacement was noted. The kernels began to show a marginal lead in horizontal displacement due to its lower mass and higher drag-to-mass ratio. However, overlap in trajectories still occurred.

At 30° (Fig. 1.3): Distinction in trajectories became clearer. The kernels travelled further along the x-axis while the shells dropped earlier. This separation indicated effective utilization of drag force differences. At 40° (Fig. 1.4): The spatial separation became even more distinct. Kernels, nuts, and shells had well-separated landing zones, validating the hypothesis that drag interaction over longer flight times enhances separation. At 45° (Fig. 1.5): While total range peaked, overlap between kernels and nuts occurred again. Due to symmetry in projectile motion and longer hang time, the nuts travelled nearly as far as the kernels. Shells still dropped earlier. It was observed that at 10 m/s, 30° to 40° offered the best compromise between horizontal displacement and separation clarity. 45° had the longest range but reduced differentiation between nuts and kernels. See table 1.1

For Velocity =10m/s, the graphical results are:

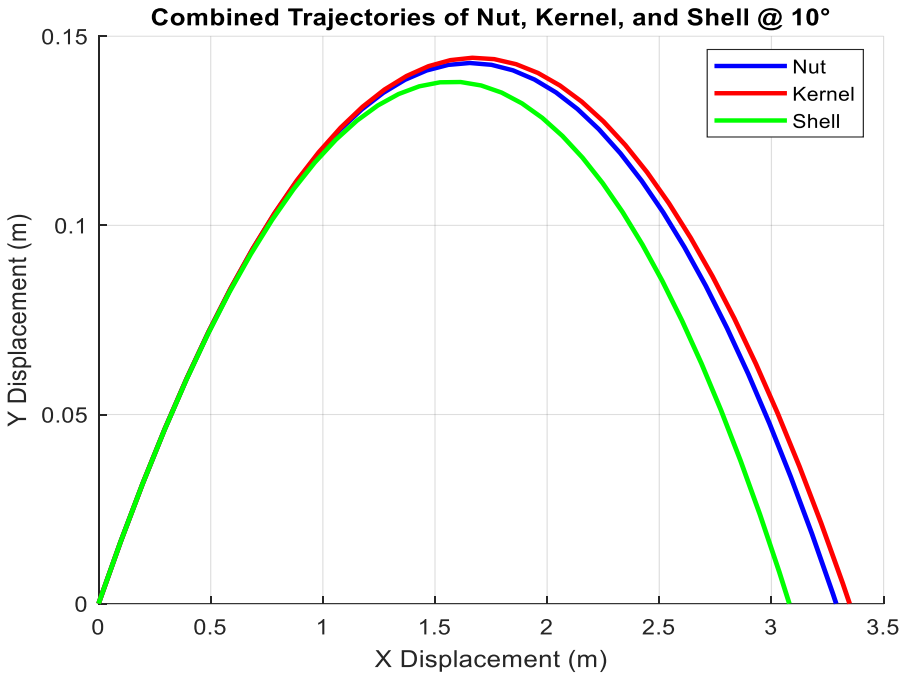

Fig. 1.1: Combined Graph of y displacement in respect to x displacement for Nut, Kernel and shell @10^0 and velocity = 10m/s

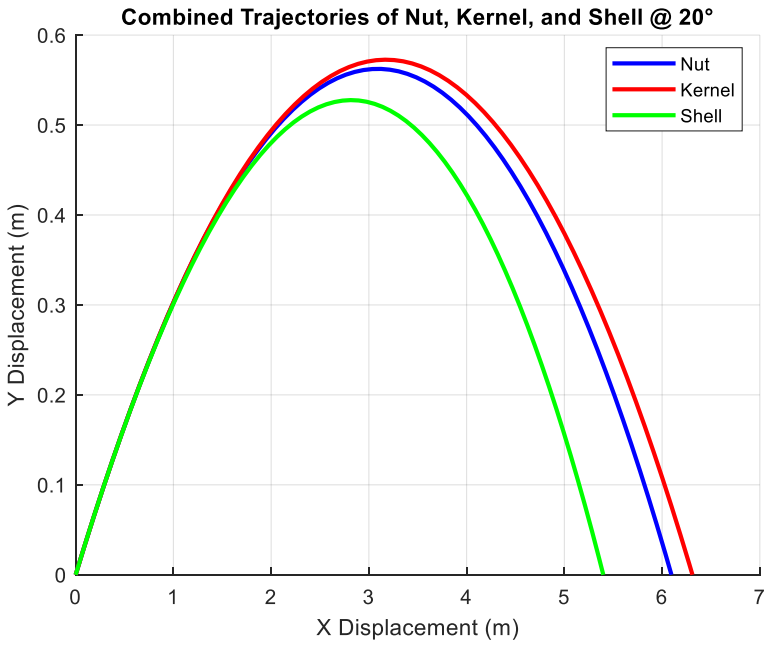

Fig. 1.2: Combined Graph of y displacement in respect to x displacement for Nut, Kernel and shell @ 20^0 and velocity = 10m/s

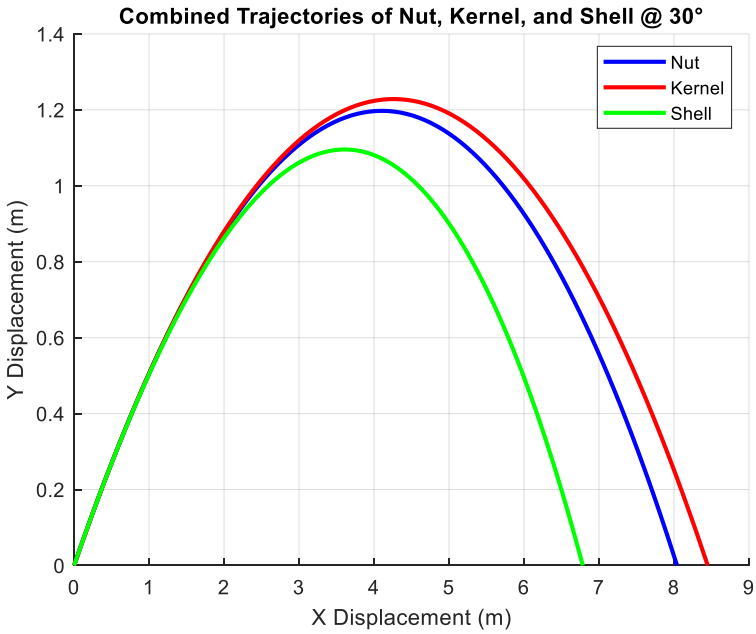

Fig. 1.3: Combined Graph of y displacement in respect to x displacement for Nut, Kernel and shell @ 30^{0} and velocity = 10m/s

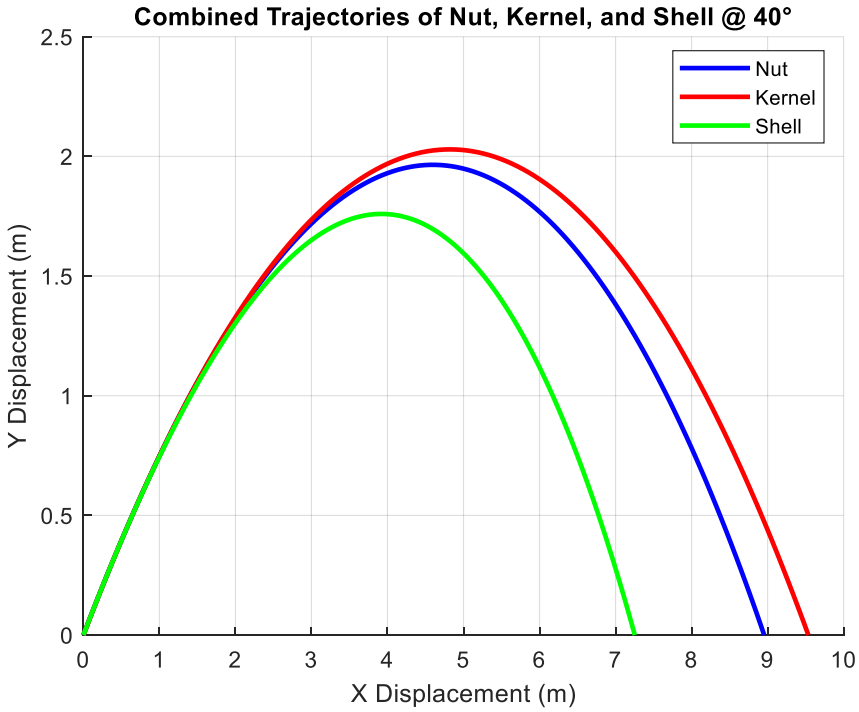

Fig. 1.4: Combined Graph of y displacement in respect to x displacement for Nut, Kernel and shell @40^{0} and velocity = 10m/s

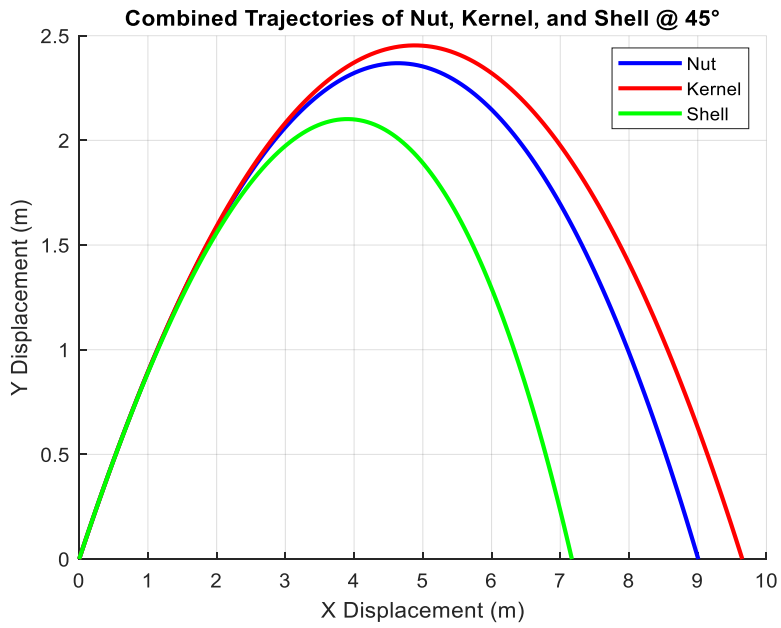

Fig. 1.5: Combined Graph of y displacement in respect to x displacement for Nut, Kernel and shell @45^0 and velocity = 10m/s

Table 1.1: The separation distances for various angles of inclination and speeds

Angle (Deg.)	Speed (m/s)	Separation/Displace met Distances (m)		
		Kernel	Nut	Shell
10	10	3.35	3.29	3.07
20	10	6.29	6.14	5.43
30	10	8.43	8.0	6.8
40	10	9.5	9.0	7.2
45	10	9.6	9.0	7.15
10	15	7.5	7.3	6.75
20	15	14.0	13.5	11.5
30	15	18.75	17.5	13.8
40	15	21.5	19.0	14.2
45	15	22	19	14.3

These graphical analyses show that as both velocity and angle increased, the separation between nut, kernel, and shell improved. However, higher angles (especially 45°) result in greater trajectory spread, which requires more space. The optimal condition balancing clear separation with minimal space requirement occurs at 30° and 15 m/s. At this point, the kernel and shell follow distinct paths without excessive displacement, making it the most space-efficient setup for effective separation.

When initial velocity was increased to 15 m/s: At 10° (Fig. 1.6): Horizontal range increased, but separation was minimal. Shells, nuts and kernels landed in a narrow band. At 20° (Fig. 1.7): Kernels began to separate more distinctly; however, drag at higher speed made shells fall short significantly. At 30° (Fig. 1.8): Optimal separation was observed. Kernels achieved longest trajectory, nuts landed mid-way, and shells dropped early, the ideal condition for a separation unit. At 40° (Fig. 1.9): Kernel range increased further but with overlap with the nuts. More vertical hang time caused convergence in mid-air paths. At 45° (Fig. 1.10): Again, though the kernels reached farthest range, both nuts and kernels shared overlapping arcs. It was observed that at 15 m/s, 30° clearly produced

the best spatial separation, optimizing the drag interaction while maintaining distinct flight paths. The data from table 1.1 were fitted to a polynomial equation and both the resulting polynomial equations and their goodness of fit, R^2, were summarized on tables 1.2 and 1.3. The maximum displacements were also indicated.

For Velocity = 15m/s, the combined graphical results

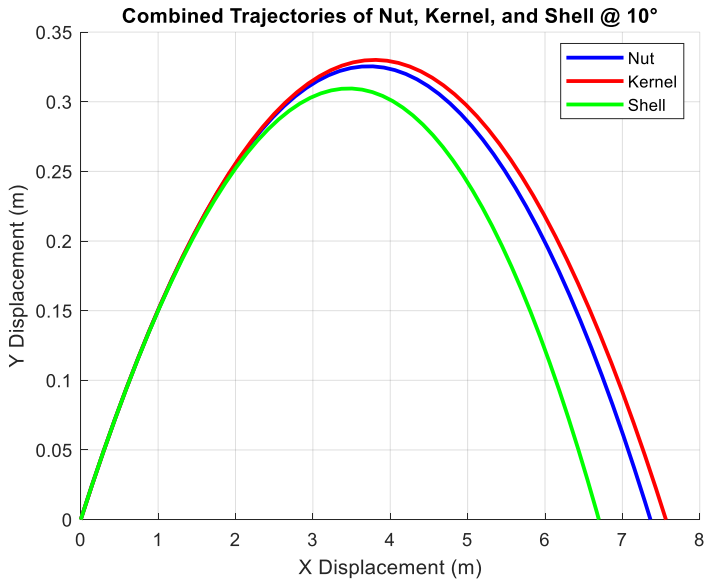

Fig. 1.6 Combined Graph of y displacement in respect to x displacement for Nut, Kernel and shell @10^0 and velocity = 15m/s

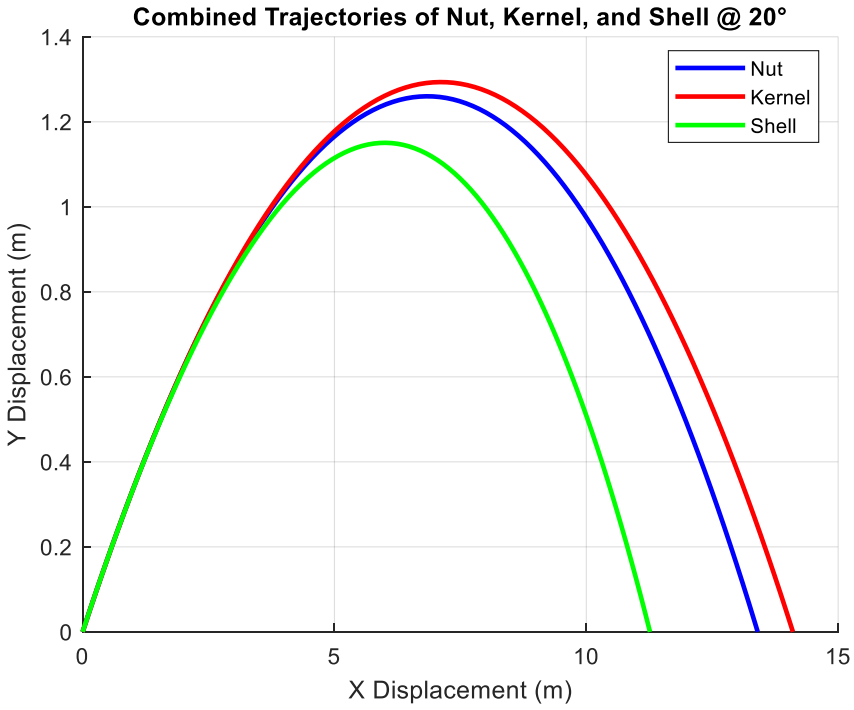

Fig. 1.7 Combined Graph of y displacement in respect to x displacement for Nut, Kernel and shell @20^0 and velocity = 15m/s

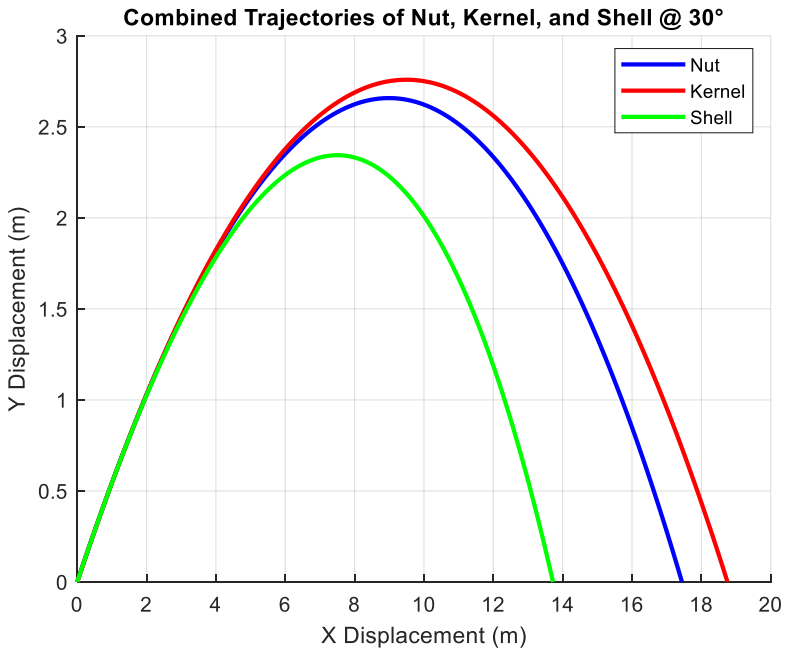

Fig. 1.8 Combined Graph of y displacement in respect to x displacement for Nut, Kernel and shell @30^0 and velocity = 15m/s

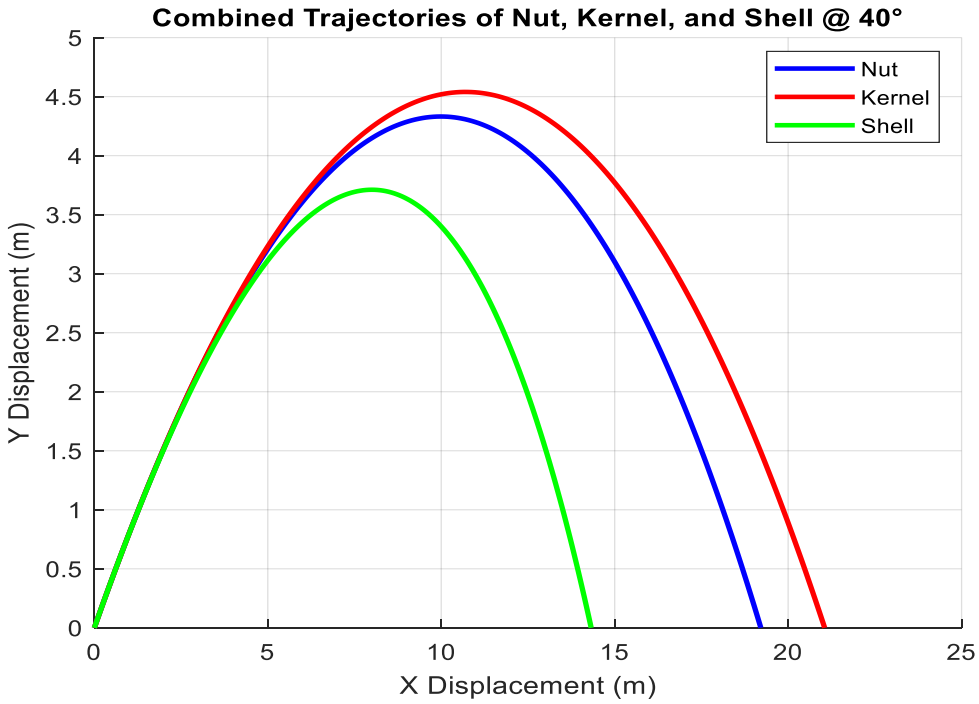

Fig. 1.9 Combined Graph of y displacement in respect to x displacement for Nut, Kernel and shell @40^0 and velocity = 15m/s

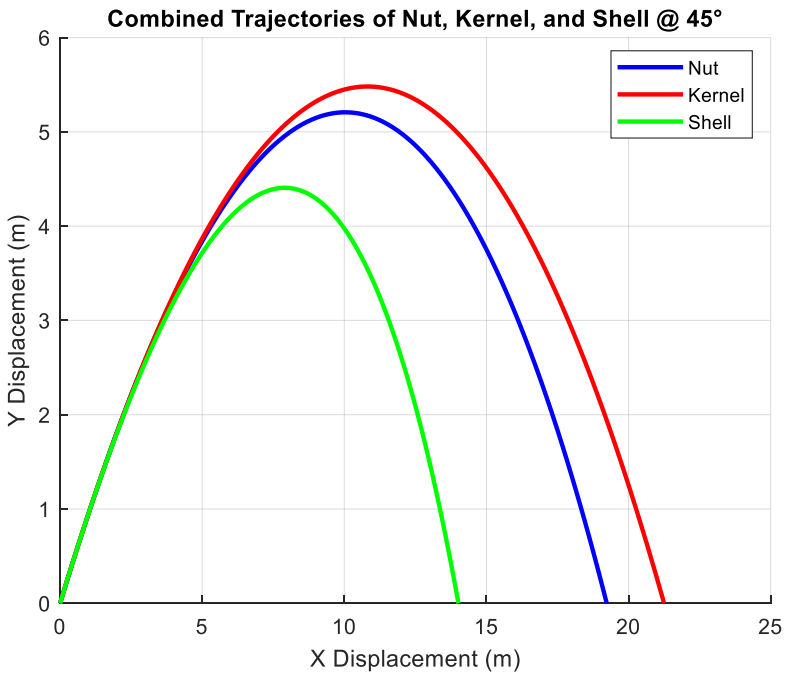

Fig. 1.10 Combined Graph of y displacement in respect to x displacement for Nut, Kernel and shell @45 ^{0} and velocity = 15m/s

Table 1.2 Summary of data from table 1.1

Material	Speed (m/s)	Equation	R^2	Maximum Displacement (m) @ 45^{o}
Kernel	10	$d = -0.6777+0.4493\theta-0.0049\theta^2$	0.9997	9.6
	15	$d = -1.0803+0.9524\theta-0.0097\theta^2$	0.9999	22.0
Nut	10	$d = -0.5436+0.4315\theta-0.0049\theta^2$	0.9998	9.0
	15	$d = -1.2662+0.9719\theta-0.0116\theta^2$	0.9999	19.0
Shell	10	$d = -0.1828+0.3733\theta-0.0047\theta^2$	0.9997	7.15
	15	$d = -0.5068+0.7287\theta-0.0095\theta^2$	0.9957	14.3

Table 1.3 Graphical Summary of Nuts, Kernels, and Shells Displacement vs Angle & Velocity

Fig. No.	Velocity (m/s)	Angle (Deg.)	Separation Observed	Trajectory Overlap	Space Efficiency	Comments
Fig. 1.1	10	10	Poor	High	Inefficient	Overlap in paths, poor separation
Fig. 1.2	10	20	Slight improvement	Moderate	Moderate	Kernel starts diverging
Fig. 1.3	10	30	Fair	Less	Better	Kernel and shell show different paths
Fig. 1.4	10	40	Good	Low	Efficient	Clear separation begins
Fig. 1.5	10	45	Very good	Very low	Less efficient	Excellent separation, but needs more space
Fig. 1.6	15	10	Slight	Moderate	Moderate	Increased velocity helps

Fig. No.	Velocity (m/s)	Angle (Deg.)	Separation Observed	Trajectory Overlap	Space Efficiency	Comments
			improvement			slightly
Fig. 1.7	15	20	Moderate	Less	Better	Improved divergence
Fig. 1.8	**15**	**30**	**Good**	**Low**	**Most Efficient**	**Clear separation in minimal space**
Fig 1.9	15	40	Very good	Very low	Less efficient	More spread than needed
Fig.1.10	15	45	Excellent	None	Least efficient	Full separation, but requires large space

Velocity = 15 m/s
Inclination Angle = 30°

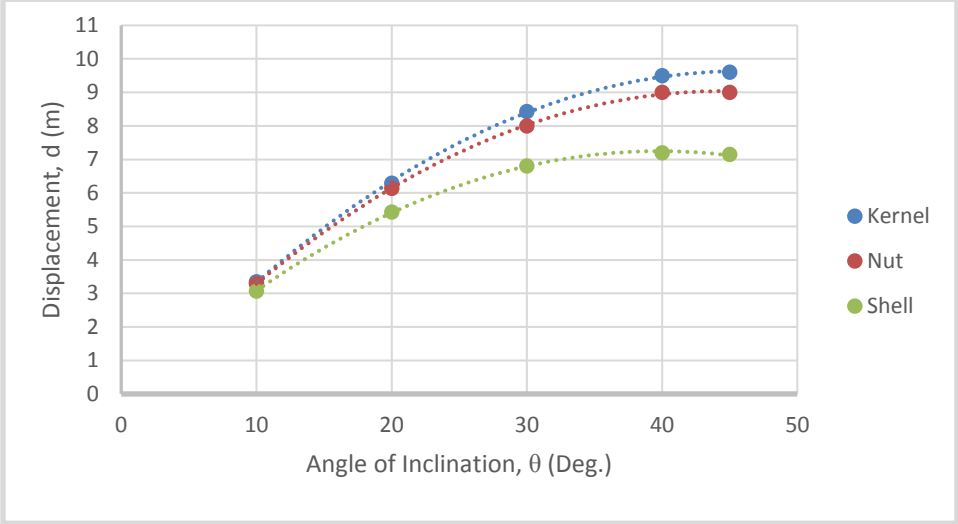

Fig. 1.11 Displacement as a function of inclination angles for speed of 10 m/s

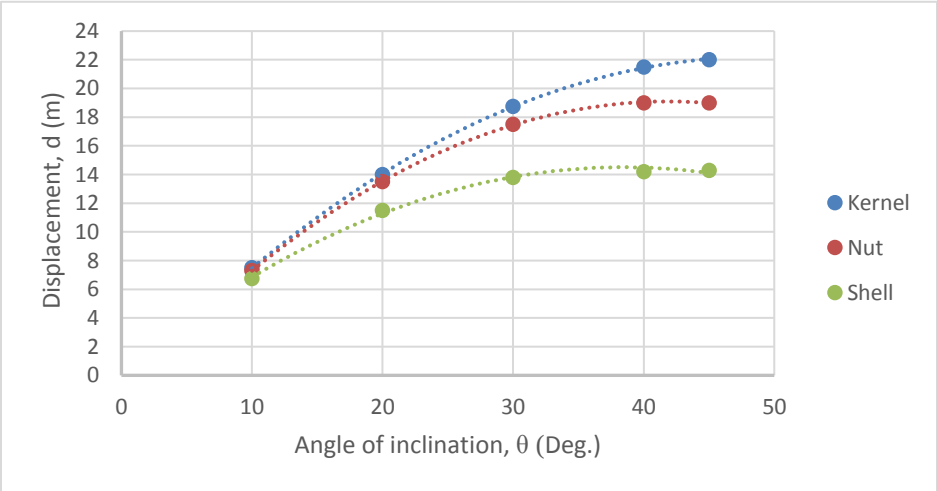

Fig. 1.12 Displacement as a function of angles of inclination for speed of 15 m/s

Table 1.4 Comparison of Theoretical and Experimental separation distances at velocity of 15m/sec and angle of inclination of 30º

Parameter	Theoretical Value (m)	Expected Theoretical Max Value (m)	Experimental value (m)
Mean Separation Distance Between Kernel and Nut	1.25	2.4919	1.372
Mean Separation Distance Between Nut and shell	3.7	4.9	3.652
Mean Separation Distance Between kernel and shell	4.95	-	5.031

4.0 Conclusion

This study developed and experimentally validated a quadratic drag–based projectile motion model for predicting the separation trajectories of palm nuts, kernels, and shells in centrifugal cracking system. Results demonstrated that aerodynamic drag plays a dominant role in post-cracking separation, particularly at discharge velocities of 10–15 m/s, where simplified drag-free models are inadequate. Both simulation and experimental findings consistently showed that separation effectiveness improved with increasing projection angles and velocities, with optimal performance achieved at a projection angle of 30° and a velocity of 15 m/s. Under this condition, kernels, nuts, and shells followed clearly distinct trajectories while maintaining minimal spatial requirements, making it the most practical configuration for industrial application.

Theoretical analysis of kernel, shell and nut motion under different ejection angles (10^0, 20^0, 30^0, 40^0, 45^0) and velocities (10 m/s and 15 m/s) (simulation), indicated that launching at 30° and 15 m/s provided the most effective separation. This optimal condition which ensures efficient categorization of the components based on flight paths was utilized for the design and development of the system whose experimental results offered efficient separation as predicted. The relationship between nuts and shells separation distances and those of kernels and nuts was described by a polynomial curve which, by curve fitting, gave an empirical relationship between these separation distances. This empirical relationship is especially useful in design to predict the separation distances for given speed/tilting angle combination.

The experimental separation distances compared with expected theoretical maximum values showed that kernel-shell separation is 98.3% efficient (using table 1.4) for projection angle of 30º and speed of 15m/s although the overall efficiency of separation between the product heaps is 63.3%. That is, the actual experimental separation distances were 63.3% of the expected theoretical maximum distances. This study provides a physics-based framework for palm kernel-shell separation by integrating quadratic air resistance into trajectory modeling and validating it experimentally. It advances existing empirical approaches by offering a predictive, explainable tool for machine design and parameter optimization, thereby reducing reliance on trial and error adjustments in separation system. Future studies should incorporate particle–particle interactions, airflow turbulence, and rotational effects to improve model fidelity. Extending the model to different palm varieties, moisture contents, and large-scale industrial separators would further enhance its applicability. The research provides linkage between projectile-drag theories and the design of agro-industrial processing equipment (agro-physics technological innovation) in which utilization of locally accessible materials guarantees the scalability.

Nomenclature

- C_D = drag coefficient (dimensionless),
- ρ = air density (kg/m³),
- A = cross-sectional area (m²),
- v = speed (m/s)

References

Adepoju, V.O., Aderinlewo, A.A., Dairo, O.U., Adetunji, O.R., & Babalola, A.A. 2023. *Determination of some physical properties of Palm Kernel and Shell in relation to frictional separation.* Journal of Natural Science Engineering and Technology, 22, 39-59.

Alade, E.I., Koya, O.A., & Omidiji, B.V. 2019. *Performance efficiency model of an integrated Palm-Nut cracker and Kernel-Shell separator*. CIGR Journal, 21(3), 218-226.

Alhaji, A.M., Almeida, E.S., Carneiro, C.R., Da Silva, C.A. S., Monteiro, S., & Coimbra, J.S. D.R. 2024. *Palm Oil (Elaeis guineensis): A journey through Ssustainability, processing, and utilization*. Foods, 13(17), 2814. Available from https://doi.org/10.3390/foods13172814

Amafade, U. G. & Ovharhea O.J.. 2024. *Oil Palm production value addition in Nigeria: The way forward*. World Journal of Advanced Research and Reviews, 21(3), 2009-2017. Available from https://doi.org/10.30574/wjarr.2024.21.3.0899

Bakri, A.J., Ajayi, T.B., Oladerin, K.O., & Mogbojuri, A.O. 2020. *Development and assessment of cracking and sorting processes of Palm Kernel Nut machine*. European Journal of Engineering Research and Science, 5(12), 145-151. Available from https://doi.org/10.24018/ejers.2020.5.12.2258

Cao, D.Q. 2023. *Separation techniques and circular economy*. Membranes, 13(9), 778. Available from https://doi.org/10.3390/membranes13090778

Diepenbroek, E., Mehta, S., Borneman, Z., Hempenius, M. A., Kooij, E. S., Nijmeijer, K., & De Beer, S. 2024. *Advances in membrane separation for biomaterial dewatering*. Langmuir, 40(9), 4545-4566. Available from https://doi.org/10.1021/acs.langmuir.3c03439

Edeh, J.C., Odunukwe, C.C., Oduma, O., & Ukwuani, T.S. 2022. *Development and evaluation of an improved inclined Belt for separating Palm Kernel and Shell*. 29(1).

Eje, B.E., Chiwetalu, U.J. and Ogbuagu, N.J. 2016. *Study of the physical properties of Palm Kernels and Shells relevant to their handling*. International Journal of Engineering, Science and Mathematics. Available from http://www.ijmra.us, p 74-75

Man, X., Li, L., Zhang, H., Lan, H., Fan, X., Tang, Y., and Zhang, Y. 2023. *Study on the relationship between crack initiation and crack bifurcation in Walnut Shells based on energy*. Agriculture, 14(1), 69. Available from https://doi.org/10.3390/agriculture14010069

Shehu, S., Salleh, M. A., & Syahadat, E. F. 2021. *The challenges facing Palm Oil industry in Nigeria*. Asian People Journal (APJ), 4(1), 26-33. Available from https://doi.org/10.37231/apj.2021.4.1.201

Taofik, O.K., Adesola, O.K., and Olatunde, A.N. 2019. *Development and performance evaluation of small-scale Palm Kernel cracker*. 2(1), 15-27.